

TRACE-METAL SOURCES AND THEIR RELEASE FROM MINE WASTES: EXAMPLES FROM HUMIDITY CELL TESTS OF HARD-ROCK MINE WASTE AND FROM WARRIOR BASIN COAL¹

S. F. Diehl², K.S. Smith, G.A. Desborough, W.W. White, III, K.A. Lapakko, M.B. Goldhaber,
and D.L. Fey

Abstract. To assess the potential impact of metal and acid contamination from mine-waste piles, it is important to identify the mineralogic source of trace metals and their mode of occurrence. Microscopic analysis of mine-waste samples from both hard-rock and coalmine waste samples demonstrate a microstructural control, as well as mineralogic control, on the source and release of trace metals into local water systems. The samples discussed herein show multiple periods of sulfide mineralization with varying concentrations of trace metals.

In the first case study, two proprietary hard-rock mine-waste samples exposed to a series of humidity cell tests (which simulate intense chemical weathering conditions) generated acid and released trace metals. Some trace elements of interest were: arsenic (45-120 ppm), copper (60-320 ppm), and zinc (30-2,500 ppm). Untested and humidity cell-exposed samples were studied by X-ray diffraction, scanning electron microscope with energy dispersive X-ray (SEM/EDX), and electron microprobe analysis. Studies of one sample set revealed arsenic-bearing pyrite in early iron- and magnesium-rich carbonate-filled microveins, and iron-, copper-, arsenic-, antimony-bearing sulfides in later crosscutting silica-filled microveins. Post humidity cell tests indicated that the carbonate minerals were removed by leaching in the humidity cells, exposing pyrite to oxidative conditions. However, sulfides in the silica-filled veins were more protected. Therefore, the trace metals contained in the sulfides within the silica-filled microveins may be released to the surface and (or) ground water system more slowly over a greater time period.

In the second case study, trace metal-rich pyrite-bearing coals from the Warrior Basin, Alabama were analyzed. Arsenic-bearing pyrite was observed in a late-stage pyrite phase in microfaults and microveins that crosscut earlier arsenic-

Additional Key Words: jarosite, copper, zinc, microanalysis

¹Paper was presented at the 2003 National Meeting of the American Society of Mining and Reclamation and 9th Billings Land Reclamation Symposium, Billings, MT, June 3-6, 2003. Published by ASMR, 3134 Montavesta Rd., Lexington, KY 40502.

²Sharon F. Diehl, Research Geologist, U.S. Geological Survey, Denver, CO 80225. K.S. Smith, G.A. Desborough, M.B. Goldhaber, D.L. Fey, U.S. Geological Survey, Denver, CO 80225. W.W. White, III, U. S. Bureau of Land Management, 2370 S. 2300 W., Salt Lake City, UT 84119. K.A. Lapakko, Minnesota Department of Natural Resources, Minerals Division, St. Paul, MN 55155-4045.

Proceedings American Society of Mining and Reclamation, 2003 pp 232-253
DOI: 10.21000/JASMR03010232

<https://doi.org/10.21000/JASMR03010232>

poor forms of pyrite. Under the scanning electron microscope, veins filled with arsenic-bearing pyrite were more pitted and dissolution etched than arsenic-poor veins, which suggests greater dissolution of the arsenic-bearing pyrite. In addition, etched weathered arsenic-bearing pyrite was depleted in arsenic content compared to adjacent unweathered arsenic-bearing pyrite.

In both cases, the characterization of microstructural properties as well as identifying the minerals enriched in trace metals and their timing of emplacement, were useful tools in predicting the amount and timing of trace element release into the local environment.

Introduction

Hard-rock mining and coal mining may generate pollutants such as high acidity, copper, iron, zinc, and arsenic and introduce these constituents at toxic levels into local environments. In two studies of sulfide-bearing mine-waste material, one collected from an exposed coal-mine face, and another collected from a hard-rock mine open pit, microscopic mineralogic analysis was key to determining the potential of mine-waste materials to generate acidic, metal-rich drainage. It is important to identify the mode of occurrence of potentially toxic trace metals, their mineralogic residence, and the ease of metal release into solution. In mine waste piles, there may be considerable void space between mined rock material that allows air and water infiltration, and hence, oxidation of the surface of the rock fragments. However, fluid infiltration into rock and the pathways of the fluids are essentially controlled by the microstructure within the rock fragments. To determine the chemical control on sulfide oxidation in waste piles, it is necessary to know the geologic materials comprising the mine waste pile, their physical properties, and the deformation history recorded in the rock. Microfractures, microveins, cracks between grain boundaries, are all viable pathways for solutions to infiltrate into rock. These pathways will control access of oxygen and water into mine waste on a microscopic scale, where chemical processes will break down sulfide minerals and generate acidic conditions and release metals into surface and ground waters.

Case Study 1: Examination of Hard-Rock Material
Subjected to Humidity Cell Tests

Samples and Methods; Humidity Cell Tests of Hard-Rock Material

Humidity cell tests are an aid for predicting acid generation during long-term weathering. These tests provide leachates for analysis of chemical products generated from mine waste (ASTM, 1996; Morin and Hutt, 1998; Lapakko and White, 2000; White and Lapakko, 2000). Two proprietary samples (numbers 81196 and 99.1) were tested in flow-through humidity cells over a period of several years (Figs. 1A, 1B). Early elemental analysis of solutions may record the dissolution of previous oxidation products in mine waste; therefore, an extensive experimental period is required to determine the rate of leaching reaction and sulfide oxidation products. A fixed volume of deionized water was dripped into each humidity cell containing a rock sample, and the resulting leachate was tested for pH and selected chemical analyses on a weekly basis (White and Lapakko, 2000). Data used to generated graph Figures 2, 3, and 6 are in Lapakko (1999).

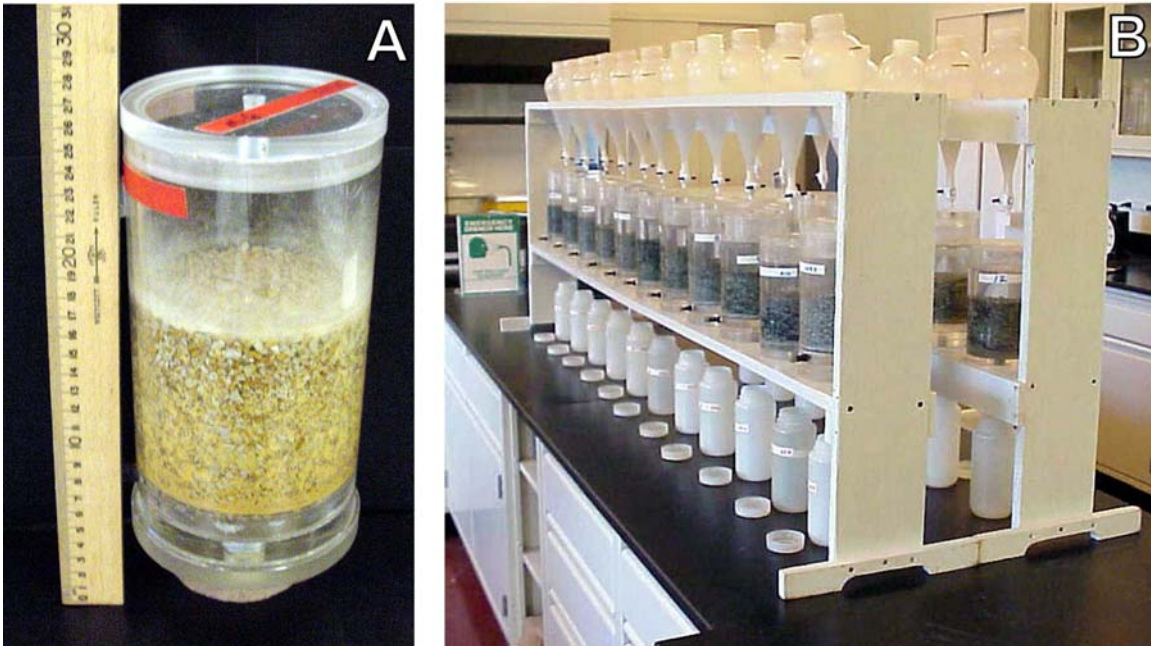


Figure 1. A. Flow-through humidity cell containing mine material. B. Humidity cell array.

In addition to studies of solution chemistry, polished thin sections of pre- and post-humidity cell test material were examined using the JEOL 5800-LV scanning electron microscope (SEM), employing both secondary electron (SEI) and back scatter (BS) imaging, to determine the character of the mineral suite. The energy dispersive x-ray spectrometer (SEM/EDX) was used to determine basic mineralogy, outline structural features, and collect semi-quantitative analyses of trace-element content. Qualitative map analyses were performed on a JEOL 8900 electron microprobe (EPMA) to determine the spatial distribution of sulfur, iron, and associated zinc, copper, and arsenic in sulfide minerals and microstructures. The operating conditions were 15 kV accelerating voltage, 20 nA (cup) primary beam current. Mineral standards were used to calibrate the instrument.

X-ray diffraction (XRD) analysis was used to determine the abundance and presence of mineral species (Table 1). Samples were prepared in a micronizing mill to an average grain size of about 5 micrometers. An internal standard of Al_2O_3 was added to help in the quantification of amorphous material. The subsequent quantitative refinements were carried out using the SIROQUANT Rietveld full-profile phase quantification program, v. 2, 1997 (Taylor, 1991). This is a quantitative method but for this study, due to the presence of clay material and solid solution minerals, numbers are reported as semi-quantitative (RSD \pm 10-15% of the value reported). Other mineral species too low in abundance to be detected by XRD, such as calcite and dolomite, were detected by SEM/EDX and (or) identified by petrographic microscopy.

Results

Geochemical Results of Humidity Cell Experiments. Leachate solutions collected from the humidity cells over a period of several years were analyzed for pH (Figs. 2A, 2B) and major elements (Figs. 3A, 3B). In the pyrite-rich sample (99.1), acidic solutions appear to be neutralized by carbonate minerals. Scanning electron microscope (SEM/EDX) studies indicate that siderite (Table 1) is accompanied by dolomite, calcite, and magnesium-rich calcite; all of which act as acid neutralizers and are present as vein-filling minerals. Initial acid solutions at pH 3.7 were quickly neutralized in the first two weeks of testing to a pH range from 5.4 to 6.4 (Fig. 2A). Carbonate neutralizers were consumed, however, at approximately 50 weeks, and then the pH of the solutions from the humidity cells dropped to about 4.5, and at the end of 94 weeks, continued to exhibit a trend towards greater acidity.

Table 1. Semi-quantitative X-ray diffraction bulk mineralogy (wt. %) of samples before and after (3 years) leaching in the humidity cell. Amorphous material is a mixture of aluminum and silica.

Sample 99.1				Sample 81196			
Mineral	Before Leaching	After Leaching	Leached Elements	Mineral	Before Leaching	After Leaching	Leached Elements
Quartz	32	30		Quartz	33	32	
Amorphous	23	28		Amorphous	33	34	
Potassium Feldspar	10	13		Jarosite	16	17	K, SO ₄
Muscovite	9	7	Al, K, Si	Potassium Feldspar	15	15	
Plagioclase Feldspar	8	8		Muscovite	2	2	Al, K, Si
Siderite	7	0	Fe	Gypsum	1	--	Ca, SO ₄
Pyrite	6	6					
Kaolinite	2	2					
Gypsum	1	3	Ca, SO ₄				

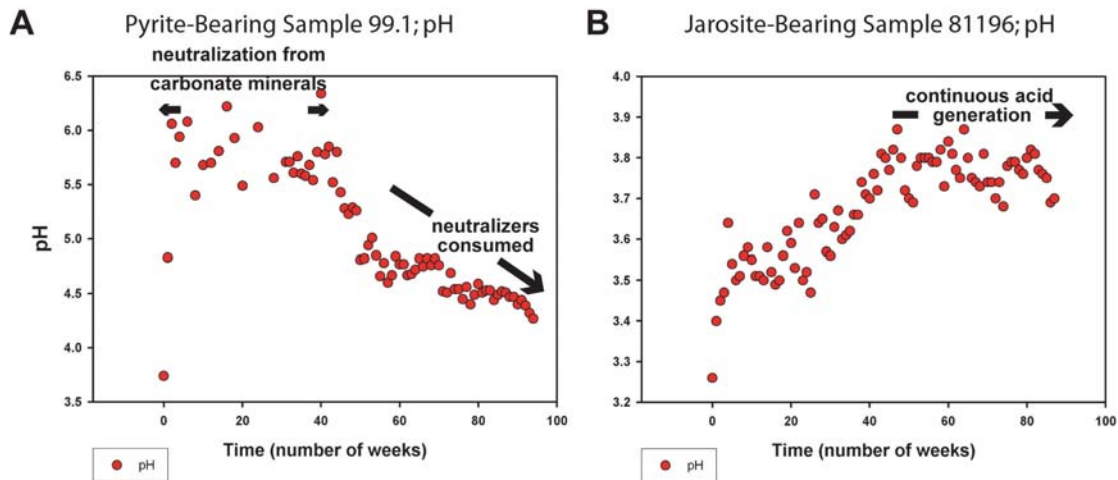
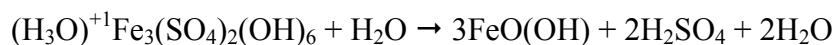


Figure 2. Plots showing pH versus time for: A. pyrite-bearing (99.1) mine sample, and B. jarosite-bearing (81196) mine sample. Sample 99.1 contains carbonate- and silica-filled veins that host sulfide minerals. Sample 81196 is an altered, weathered sample with rare, fine-grained pyrite but abundant jarosite.

In contrast, the pyrite-deficient, jarosite-rich sample (81196) continuously generated acidic solutions in the 3.6 to 3.8-pH range, even after 94 weeks of testing (Fig. 2B). Hence, it appears that the dissolution of jarosite, e.g. hydronium jarosite or potassium jarosite, produces acid:



or Stoffegren et al. (2000) suggest:



Previous studies of leachate chemistry of mine-waste samples containing jarosite and no other potential acid generator suggested that jarosite was a factor in generating low-pH conditions (Desborough et al., 1999). The solubility of jarosite, (the potassium end member) is reported by Baron and Palmer (1996); the log K_{sp} for the jarosite dissolution reaction at 25 °C is -11.0 ± 0.3 . Our studies suggest that the jarosite we observe in the humidity cell tests is undergoing dissolution.

Major Element Leachate Chemistry. Figures 3A and 3B show the leaching characteristics of several major elements. Element concentrations appear to level off after an initial decrease over time for the 25 to 50 week time period. However, there is significant continued release of the major elements even after a 4-year period in the humidity cells. For the time periods in excess of 150 weeks, there may be a slight increase of major-element leaching, especially for sample 99.1.

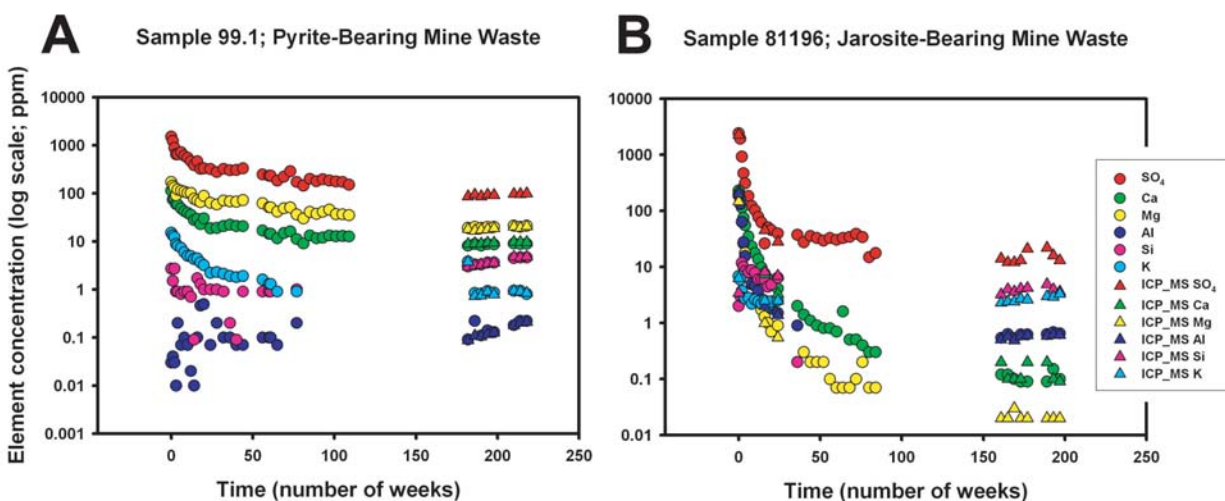


Figure 3. A. Leachate chemistry for pyrite-bearing sample 99.1. B. Leachate chemistry for jarosite-bearing sample 81196. Starting at approximately 50 weeks, the graph demonstrates a fairly stable, long-term continuous leaching of major elements into solution.

The source of Ca^{2+} in solution is problematic as the samples contain soluble sulfate minerals (Table 1) and both gypsum and calcite undergo dissolution in acidic conditions. In the first weeks of humidity cell tests, much of the Ca^{2+} is assumed to be derived from the dissolution of gypsum, especially in the case of sample 81196, in which gypsum is not detected by XRD after leaching (Table 1). This suggests that gypsum has undergone total dissolution in this sample.

However, gypsum appears to be an oxidation product in the pyrite-bearing sample 99.1 (Table 1), where gypsum increases in concentration after leaching (Table 1). Plots of Ca^{2+} versus Mg^{2+} (Figs. 3C and 3D) suggest that the two elements are strongly related; as one element increases in concentration in solution, the other does also. These data indicate that Ca^{2+} and Mg^{2+} originate from a related source, the dissolution of carbonate minerals.

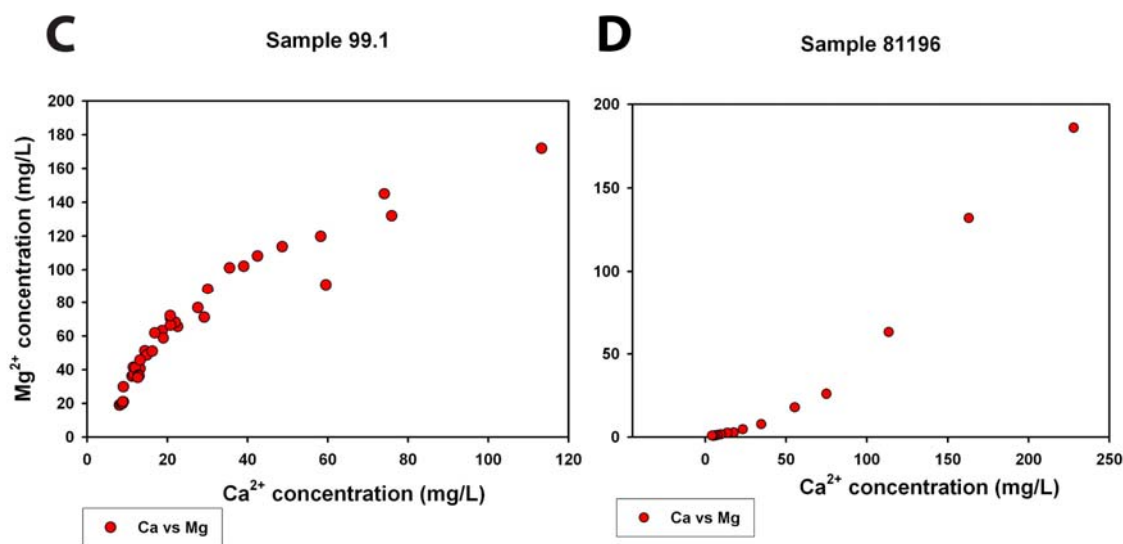


Figure 3. C. Leachate chemistry for pyrite-bearing sample 99.1. D. Leachate chemistry for jarosite-bearing sample 81196. Both samples show that as Ca^{2+} increases in solution, Mg^{2+} does also.

Structure and Mineral Textures. In addition to mineralogic differences, the two samples (99.1 and 81196) have different structural and textural characteristics. SEM analysis shows that the pyrite-bearing sample 99.1 underwent multiple periods of deformation and influx of mineralizing fluids (Fig. 4A). Early carbonate-filled veins are host to pyrite and arsenic-bearing pyrite. The carbonate-filled veins are composed of irregular bands and intergrowths of dolomite ($\text{CaMg}(\text{CO}_3)_2$), siderite (FeCO_3), calcite (CaCO_3), and magnesium-rich calcite (Ca,MgCO_3). End

members from iron-rich carbonates to magnesium-rich carbonates are present. The older carbonate-filled vein is cross cut by the younger silica-filled vein (Fig. 4A). The silica-filled veins contain the sulfide minerals pyrite, arsenic-bearing pyrite, chalcopyrite, and tennantite-tetrahedrite, a source of copper-zinc arsenic metals.

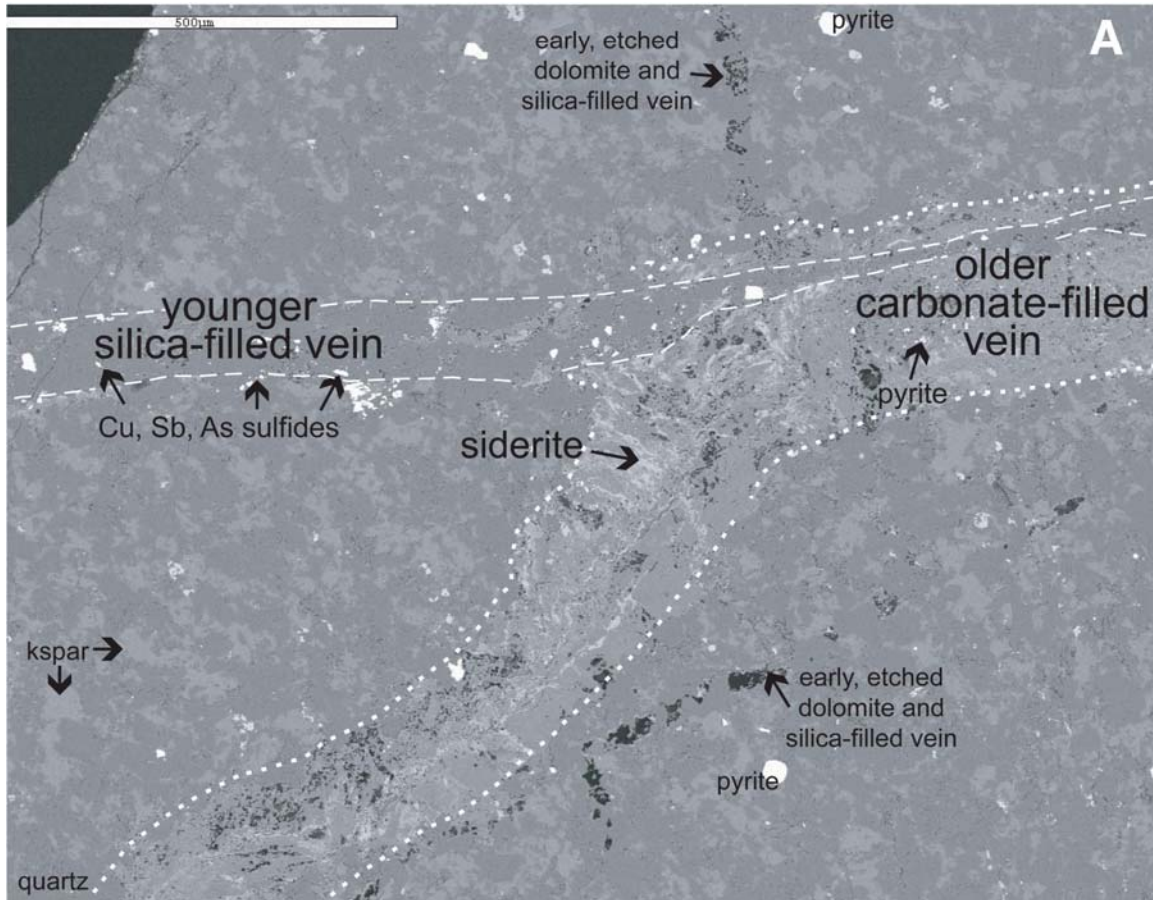


Figure 4A. Scanning electron photomicrograph of mine sample 99.1, a siltite/argillite, showing at least three periods of deformation, from oldest to youngest: (1) thin dolomite and silica-filled veins, (2) carbonate-filled veins, and (3) a silica-filled vein crosscutting the earlier carbonate vein. The carbonate and silica-filled veins contain different sulfide mineralogy. Sulfide minerals of unknown affinity with a deformation event are disseminated in the matrix of the silicified siltite/argillite.

Sulfide minerals in sample 99.1 have undergone degradation in the humidity cell tests (Figs. 4B, 4C). Pyrite in an untested sample has a fresh unfractured surface and contains inclusions of titanium oxide and quartz (Fig. 4B). In a post humidity cell test (after 3 years) sample, pyrite is

partially oxidized, dissolved, and fractured (Fig. 4C), but abundant pyrite remains as a potential source of acid.

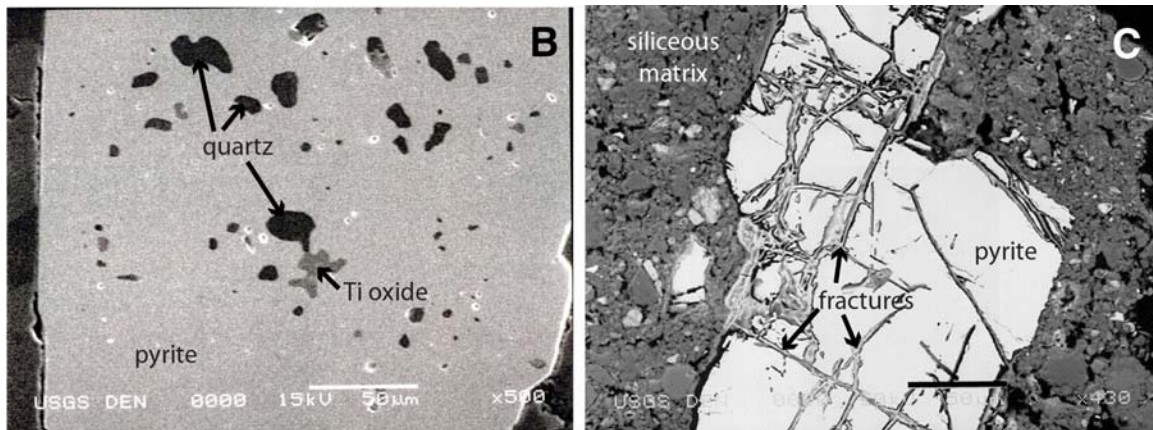


Figure 4B. Scanning electron photomicrograph of pyrite before the humidity cell test. The pyrite grain has inclusions of quartz and titanium oxides. C. Pyrite after 2 years in the humidity cell test. The pyrite is partially dissolved and highly fractured. Note that fluids will more easily flow into and interact with the pyrite shown in C.

Microprobe element maps show that sulfide minerals in the carbonate-filled veins have low concentrations of trace metals such as copper, zinc, and arsenic, whereas sulfide minerals in the silica-filled veins have high concentrations of copper, zinc, and arsenic (Fig. 4D).

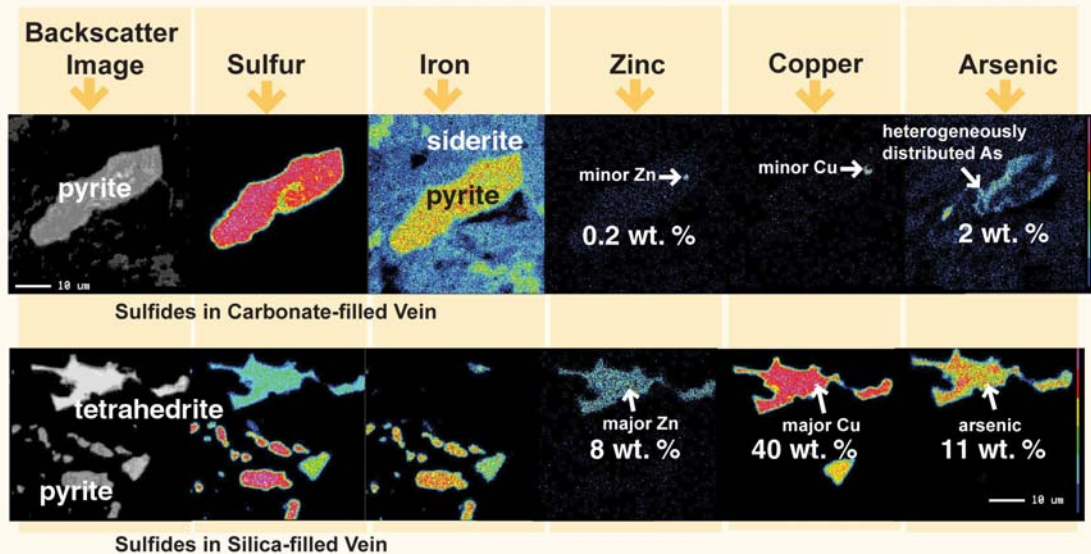


Figure 4D. Scanning electron backscatter photomicrographs of pyrite in a carbonate-filled vein (top part of photo) and sulfide minerals in a silica-filled vein (lower half of photo). From left to right, backscatter images of the sulfide minerals are followed by microprobe element maps of sulfur, iron, zinc, copper, and arsenic. Cool, blue colors indicate low concentrations of elements; warm, yellow to red colors indicate higher concentrations of elements. Weight percentages of elements are from semi-quantitative SEM/EDX analysis. Note that sulfide minerals in the carbonate-filled veins have low concentrations of trace metals, such as copper, zinc, and arsenic, whereas sulfide minerals in the silica-filled veins have high concentrations of copper, zinc, and arsenic.

The (pre-leached) jarosite-bearing sample, 81196, is a more highly altered and porous rock than the veined sample, 99.1 (Fig. 5A). Alteration minerals, such as mica and jarosite, have open porous textures. Micaceous alteration products (sericite?) and iron oxides (Fig. 5B) embay quartz and feldspar grains. The micaceous minerals have open cleavage or fractures, and the jarosite has undergone partial dissolution along chemically distinct zones (Fig. 5C, 5D). Copper resides in the outer zone of some jarosite crystals (Fig. 5D).

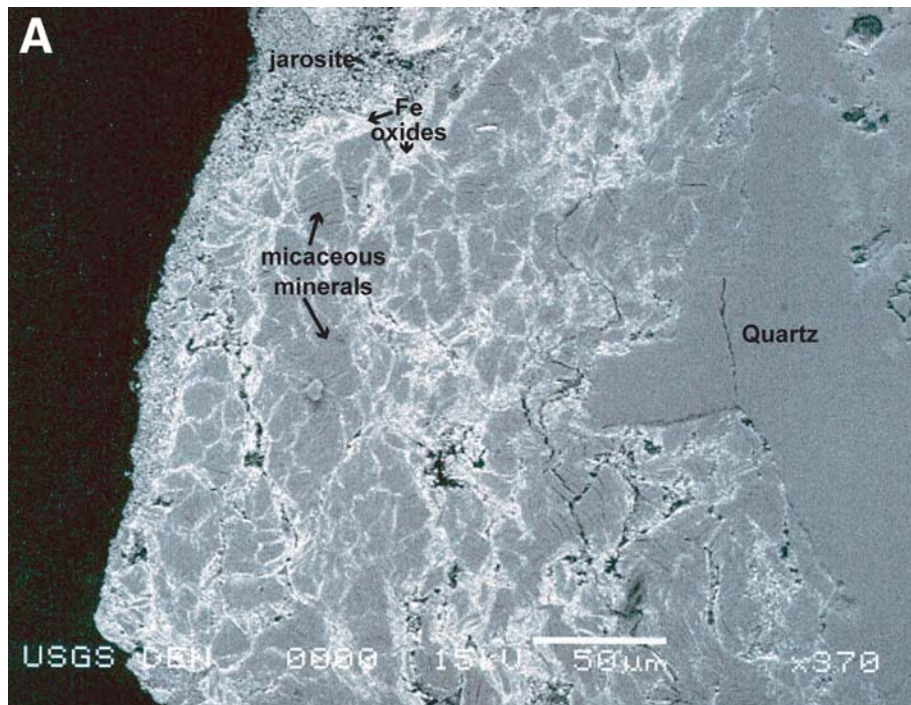


Figure 5A. Scanning electron photomicrograph of jarosite-bearing sample 81196. This mine sample contains products of weathering—micaceous minerals, jarosite, and iron oxides. These minerals formed in situ and not as a result of the humidity cell test. These minerals exhibit porous textures, open to percolating solutions. They have high ion exchange capacity and are capable of sorbing trace metals.

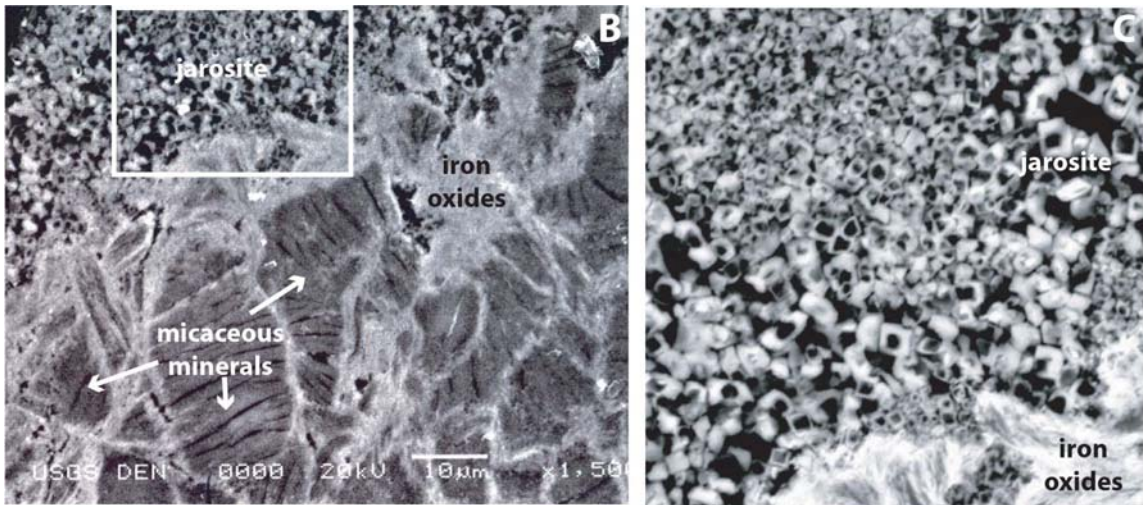


Figure 5B. Scanning electron photomicrograph of a polished surface of sample 81196, showing micaceous minerals, iron oxides, and jarosite. Open cleavage planes are evident in the mica. Iron oxides are an alteration product surrounding and coating the mica. Jarosite, also an alteration product, coats rock fragments. C. Scanning electron photomicrograph of the area outlined in the white rectangle in B. Jarosite exhibits hollow centers, probably due to dissolution of a precursor mineral phase. No clay minerals were detected in 81196.

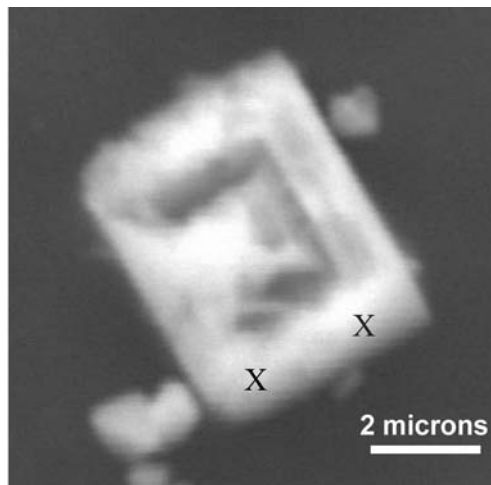


Figure 5D. Scanning electron photomicrograph of a jarosite crystal (unpolished 3-dimensional sample) in sample 81196. Jarosite crystals exhibit a chemical zonation, evidenced here by dissolution of the core of the crystal and partial dissolution of one or more zones. Up to 0.68 wt. % Cu was detected (semi-quantitative SEM/EDX) in the outermost zone (marked by X's).

Geologic Controls of Trace-Element Chemistry. The mine samples exhibit several crosscutting deformation events that introduced different generations and types of mineralization. Pyrite in the older carbonate-filled veins has low concentrations of the trace metals copper, zinc, and arsenic. Sulfide minerals in the younger silica-filled veins contain higher concentrations of copper, zinc, and arsenic (Fig. 4D). In an acidic environment, the carbonate minerals will dissolve first, exposing sulfide minerals to oxidative conditions, and releasing the trace metals into solution. Because silica is less soluble, trace metals in the sulfides in the silica-filled veins will be released more slowly from mine waste over a longer time period. This is demonstrated in plots of leachate chemistry of copper and zinc from both the pyrite- and jarosite-rich samples (Figs. 6A, 6B). Even after 4 years in a humidity cell, there is metal release into solution from both samples. However, the pyrite-bearing sample (99.1) shows an increase in concentration of copper and zinc going into solution at about 200-weeks.

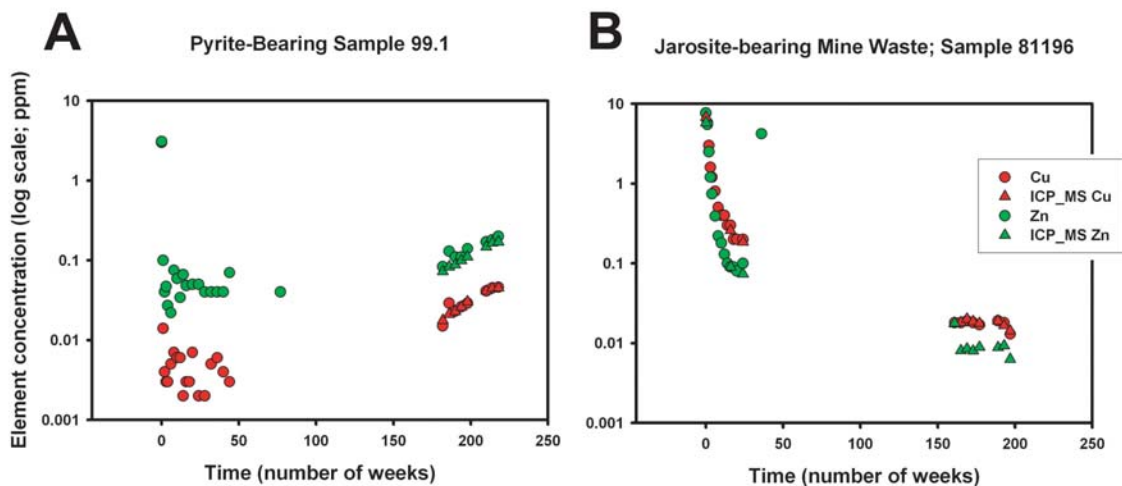


Figure 6. Plots of copper and zinc concentration versus time in leachates from humidity cells in a four-year test period. A. The concentration of copper and zinc in solution increases at around 190 weeks. B. Copper and zinc are leached from the jarosite-rich samples after a four-year period, but concentration levels drop at around 200 weeks.

Discussion

Even though pyrite in sample 99.1 was partially dissolved during humidity cell tests, most of the pyrite was still present after several years. In a mine-waste pile, oxidation of this sulfide

mineral would continue to generate acid for many years to come. Furthermore, Figure 6A demonstrates that trace metals continue to be released from this mine material under oxidative conditions.

The solubility of the different vein-filling minerals that contain the metal-bearing sulfide minerals may be a factor in the continuous release of trace metals. Carbonate minerals are soluble at low pH, therefore the carbonate-filled veins probably experienced rapid dissolution upon leaching, but the leached fluids contained relatively low trace element concentrations. Silica is less soluble at low pH, therefore the silica-filled (quartz) veins experienced slow dissolution upon initial leaching. The tight structure of siliceous veins, and the fact that silica acts as an armor around the sulfide minerals under acidic conditions, prevents the oxidation of trace-metal-bearing sulfide minerals early in the humidity cell test. Leachate fluids from sulfides exposed in the silica-filled veins are relatively high in trace element concentrations at the end of the humidity cell test (Figs. 3A, 6A). This suggests that the silica-filled veins eventually decrepitate only after a longer time in the humidity cell and at higher pH.

Conclusions

Geochemical results from humidity cell tests demonstrate that trace elements are leached from mine waste materials in the humidity cell tests. Trace elements may be transported into surface and ground waters, accumulating in stream sediments and in soils.

Mineralogy, structure, and texture controlled leachate chemistry in the humidity cell tests. The jarosite-rich, pyrite deficient sample (81196) continuously produced acid upon leaching in the humidity cell, suggesting that jarosite is the source of the acid.

Geochemical analyses show that carbonate-filled veins dissolve more readily under acid conditions than do the silica-filled veins. Therefore, the solubility of vein-filling minerals is a control on the timing of the release of trace metals into the environment.

Case Study 2: Lost Creek Coalmine:

Introduction

Trace metals, such as copper, molybdenum, zinc, and arsenic, are present locally at elevated concentrations in coal of the Warrior Basin of Alabama (Oman et al., 1995; Goldhaber et al., 1997). These trace metals primarily reside in the mineral pyrite but are also enriched to a lesser degree in coal (Goldhaber et al., 2000). Trace metals may be released to the environment during coal mining, processing, or combustion. Soil and sediment samples collected in drainage systems near abandoned mines, such as the Lost Creek (Fig. 7), show elevated concentrations of arsenic, copper, and zinc (Goldhaber et al., 2002; Morrison et al., 2002).

Previous studies suggest that trace metals were introduced into the coal along faults and fractures (Goldhaber et al., 1997; Diehl et al., 2002). A geologic map of the Warrior Basin Coal field shows a strong northwest-southeast system of normal faults that were generated during the Alleghanian orogeny (Fig. 7) (Pashin, 1991). These faults probably acted as channels for westward migrating metal-bearing fluids.

Although coal samples were collected from several abandoned mine locations in the Warrior Coal Basin, only representative samples from the Lost Creek Mine are presented herein (Fig. 7). For a more complete listing of mines samples and data tables of the geochemistry of trace element concentrations in pyrite see Diehl et al. (2002).

Methods And Materials

Pyrite-bearing coal samples were collected from fault zones in an abandoned mine facing at the Lost Creek Mine. Pyrite-filled veins were abundant at faulted, structurally disrupted areas. Pyrite mineralization was confined to within 50 m of a fault zone. Polished coal samples were examined using both SEM/EDX, a JEOL Microprobe, and laser ablation inductively coupled plasma mass spectrometer (LA-ICP-MS; see Ridley, 2000). All methods were useful in determining the exact mineralogic residence of the trace metals. However, with the exception of arsenic, the concentration of trace metals such as copper, zinc, and lead were too low to map with the microprobe, so we determined the concentration of these elements in pyrite (Table 2)

with LA-ICP-MS, using a 25-micron beam size and the U.S.G.S. sulfide standard PS-1 as a calibration standard (Wilson et al., 2002).

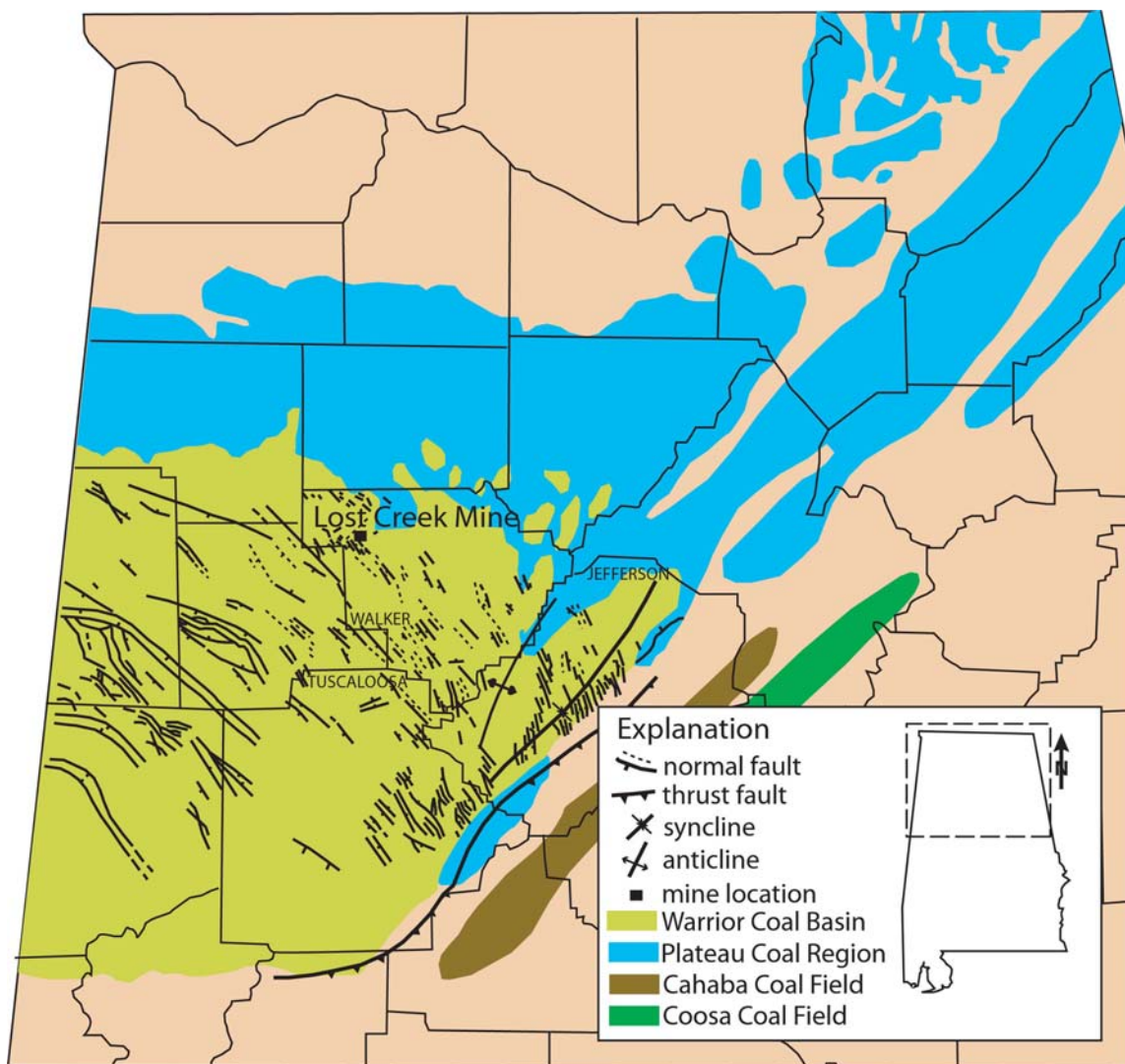


Figure 7. Location map of northern Alabama, depicting the location of Lost Creek Mine, an Alleghanian thrust fault, axes of folds, and a strong northwest/southeast trending normal fault system (after Pashin, 1991). The latter fault system was a probable fluid migration pathway for metal-bearing solutions.

Results

Pyrite mineralization in the Lost Creek sample is multigenerational. Pyrite occurs as framboids and as coarse-grained massive pyrite that fills woody cell structures and

microstructures. Framboidal pyrite is an early sulfide mineral composed of microcrystalline cubes, commonly occurring in spheres (Fig. 8A). Framboidal pyrite may be recrystallized or encased and overgrown by later generations of coarse-grained pyrite, but the framboids commonly maintain a recognizable spherical shape within the pyrite mass (Fig. 8A). Framboidal pyrite is arsenic-poor compared to the coarse-grained pyrite (Table 2) but enriched in elements such as copper, cobalt, and lead (Fig. 8B).

Table 2. Trace metal concentration (laser ablation mass spectrometer data) from selected samples of framboidal and coarse-grained pyrite in Lost Creek coal.

Sample Traverse Number; Pyrite Morphology	Co ppm	Ni ppm	Cu ppm	Zn ppm	As ppm	Mo ppm	Sb ppm	Tl ppm	Pb ppm
29 framboid	75	112	7	0	660	7	0	3	3
30 framboid	100	130	6	0	501	5	1	3	4
31 coarse-grained	6	0	2	0	1985	10	0	4	0
32 coarse-grained	2	0	0	0	4571	4	0	4	0.3
33 framboid	138	156	3	67	240	11	1	2	4
34 framboid	98	138	5	56	458	4	0.9	3	3
35 coarse-grained	0	0	0	0	2050	10	0	2	0.2
36 coarse grained	0	0	0	0	7467	6	0	3	0
37 framboid	97	137	4	60	788	6	1	3	5
38 coarse grained	0	0	0	0	1978	6	0.9	8	0

Pyrite-filled veins commonly exhibit growth banding with up to 2.5-wt. % arsenic, together with contents of up to 100-ppm molybdenum, 20-ppm mercury, and 10-ppm thallium. Gold was detected in some late-stage pyrite veins at concentrations ranging from 0.001-0.3 ppm with an average of 0.05 ppm (for a complete set of data tables, see Diehl et al., 2002).

A laser ablation mass spectrometer traverse across a pyrite sample that includes both framboidal and coarse-grained pyrite shows the chemical differences between the pyrite morphologies (Table 2; Fig. 8). Early framboidal pyrite hosts trace metals that include cobalt, nickel, copper, zinc, and lead. Later coarse-grained pyrite hosts significant concentrations of arsenic, but is low in other trace metals. Arsenic-bearing coarse-grained pyrite rims are observed circumscribing some framboidal pyrite (upper left part of Fig. 8A, arsenic element map). This arsenic-bearing pyrite in turn is encased by a third generation or phase of pyrite that is less rich in arsenic (Fig. 8A).

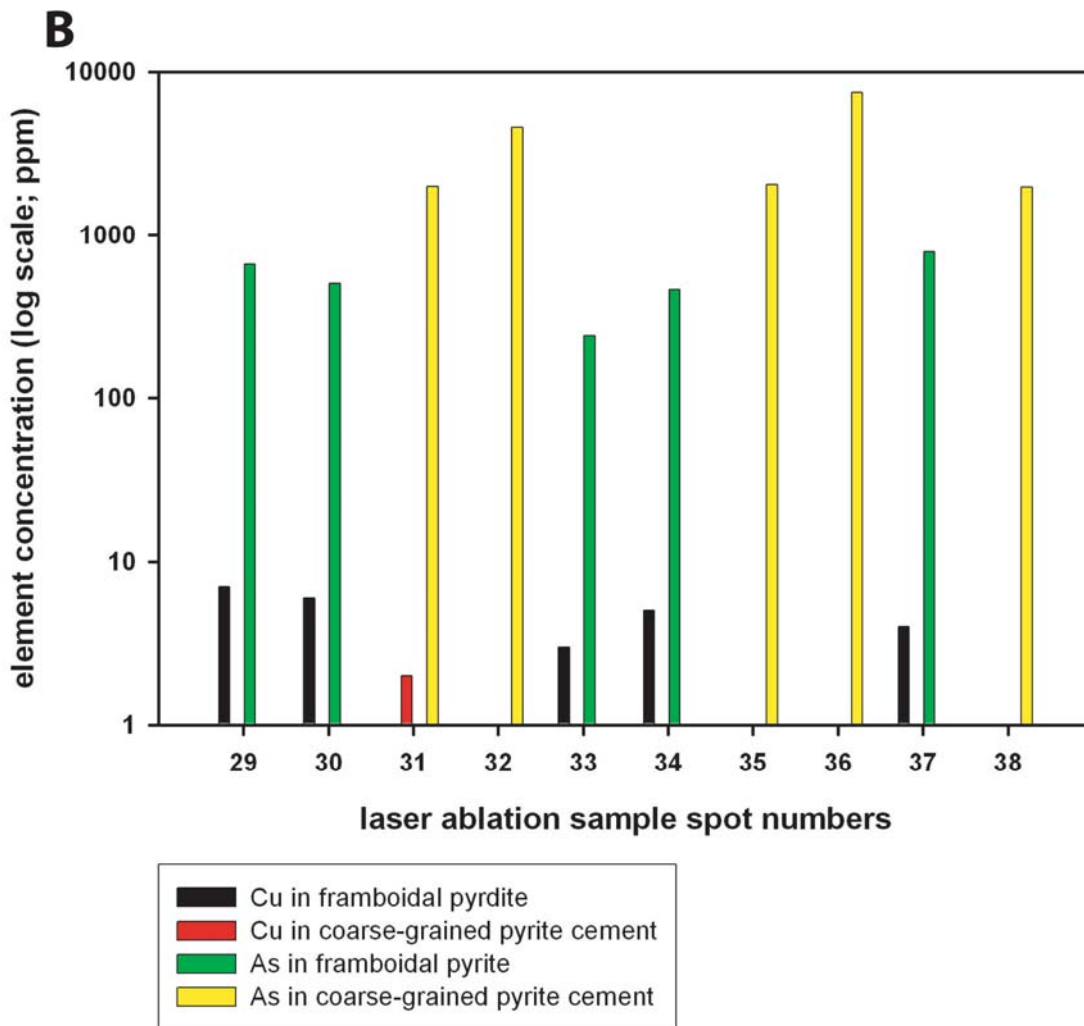
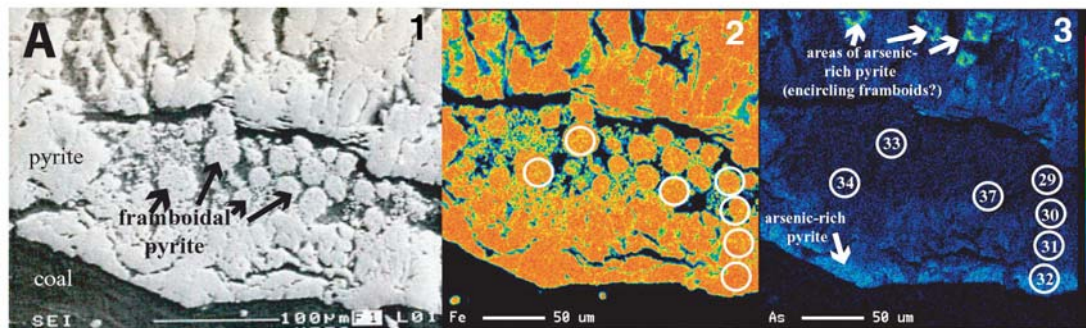


Figure 8. Lost Creek Mine sample. A. From left to right, (1) scanning electron photomicrograph of spheres of framboidal pyrite encased in later generations of coarse-grained pyrite, (2) microprobe element map of iron showing distribution of pyrite, and (3) microprobe element map of arsenic distribution in pyrite. Cool blue colors indicate low concentrations of arsenic; warmer yellow-green colors denote higher concentrations of arsenic. White circles are laser ablation sample spots (samples 35, 36, and 38, listed in Table 2, are out of the photo's view). B. Plot of copper and arsenic concentration in framboidal pyrite (black and green bars) and in coarse-grained pyrite (red and yellow bars). Note that the spheres of early-formed framboidal pyrite in the center of the photomicrographs are low in arsenic, but higher in copper compared with the coarse-grained pyrite.

Coarse-grained pyrite in the cell structures is arsenic-poor, but successive generations of pyrite, as rims, or overgrowths, outside the cell-wall boundaries and filling microstructures, are enriched in arsenic (Fig. 9). Microveins and microfaults generated by deformation of the coal bed were evidently fluid conduits for metal-bearing solutions, as demonstrated in microprobe elemental maps that show arsenic localized along microveins and fractures that cross cut the arsenic-poor pyrite in woody cell structures (Fig. 9).

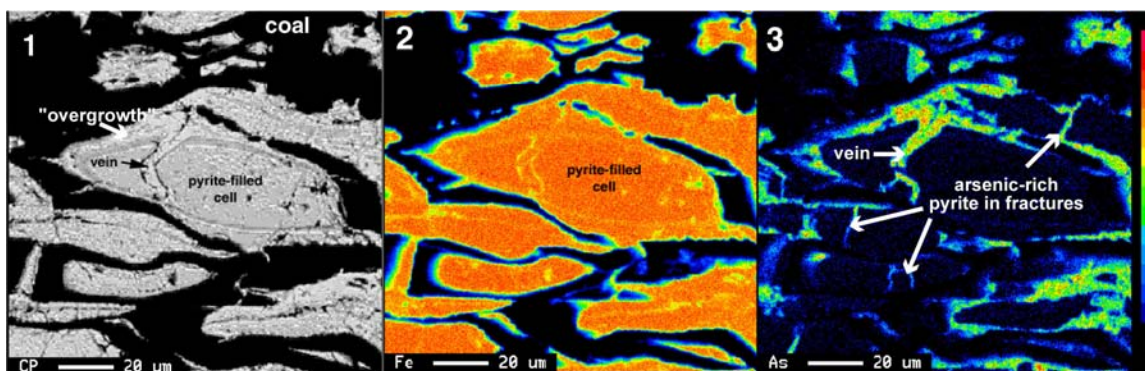


Figure 9. From left to right, (1) scanning electron photomicrograph of a pyrite-filled cell structure (in coal) with an arsenic-bearing overgrowth and crosscut by a microvein, filled by arsenic-bearing pyrite; (2) microprobe element map of iron, showing pyrite-filled cells and cell walls; and (3) microprobe element map of arsenic, showing arsenic-poor pyrite in cell structures and arsenic-bearing pyrite overgrowths/rims, as well as arsenic-rich alteration along microfractures.

Discussion and Conclusions

On a macroscopic scale, arsenic-bearing pyrite is associated with faults related to Alleghanian tectonism (Diehl et al., 2002; Goldhaber et al., 2002). On the microscopic scale, arsenic-bearing pyrite clearly postdates early diagenetic sulfides such as framboids and cell-filling pyrite. Even though mining operations generally avoid the pyrite-rich faulted zones, these areas of sulfides enriched in arsenic are left exposed to erosion and weathering processes.

In terms of environmental impact, the primary result of the coal study is that potentially toxic trace elements are concentrated in the mineral pyrite. Furthermore, much of this arsenic-bearing pyrite in Warrior Basin coal tends to be coarse grained and susceptible to removal by coal-cleaning procedures. Coarse-grained pyrite may be easily milled from coal, but the fine-grained framboidal pyrite with its higher trace metal content is problematic.

Summary

Both hard-rock and coalmine waste piles commonly contain abundant non-ore sulfide and sulfate minerals that are sources of metal contamination to local water supplies. Metals may be leached from mine waste at harmful levels to aquatic and land-based wildlife.

To control trace-metal release from mine waste, it is imperative to understand the mode of occurrence and the mineralogic residence of the trace metals. Microprobe element maps demonstrate that potentially toxic trace metals, such as arsenic, copper, and zinc, have heterogeneous distributions in host sulfide minerals. SEM and humidity cell tests demonstrate that structural elements in mine waste rock fragments, and not just the solubility properties of individual minerals, exert a control on release of trace metals. Knowledge of the mineralogic source of potentially toxic elements and of the physical properties of the host minerals may allow for better remediation approaches.

Acknowledgements

Stephen J. Sutley, U.S. Geological Survey, provided semi-quantitative X-ray diffraction data.

Literature Cited

- American Society for Testing and Materials. 1996. ASTM Designation: D 5744 - 96 - Standard Test Method for Accelerated Weathering of Solid Materials Using a Modified Humidity Cell, ASTM, West Conshohocken, PA, 13p.
- Baron, D., and Palmer, C.D. 1996. Solubility of jarosite at 4-30°C: *Geochimica et Cosmochimica Acta*, v. 60, p. 185-195. [http://dx.doi.org/10.1016/0016-7037\(95\)00392-4](http://dx.doi.org/10.1016/0016-7037(95)00392-4)
- Desborough, G.A., Leinz, R.W., Smith, K.S., Hageman, P.H., Fey, D.L., and Nash, T. 1999. Acid Generation and Metal Mobility of Some Metal-Mining Related Waste in Colorado: U.S. Geological Open-File 99-322, 18 p.
- Diehl, S.F., Goldhaber, M.B., Hatch, J., Kolker, A, Pashin, J.C., and Koenig, A.E. 2002. Mineralogic Residence and Sequence of Emplacement of Arsenic and Other Trace Elements

- in Coals of the Warrior Basin, Alabama *in* Proceedings, 19th International Pittsburgh Coal Conference, CD ROM, Section 16, Trace Metal Contamination.
- Goldhaber, M.B., Bigelow, R.C., Hatch, J.R., and Pashin, J.C. 2000. Distribution of a suite of elements including arsenic and mercury in Alabama coal: U.S. Geological Survey MF Map 2333, <http://greenwood.cr.usgs.gov/pub/mf-maps/mf-2333/>
- Goldhaber, M.B., Hatch, J.R., Pashin, J.C., Offield, T.W., Finkelman, R.B. 1997. Anomalous arsenic and fluorine concentrations in carboniferous coal, Black Warrior Basin, Alabama: Evidence for fluid expulsion during Alleghanian thrusting: Geological Society of America, Abstracts with Programs, Annual Meeting, v. 29, no. 6, p. A51.
- Goldhaber, M.B., Lee, R., Hatch, J., Pashin, J., Treworgy, J. 2002. The role of large-scale fluid flow in subsurface arsenic enrichment *in* Stollenwerk, K., and Welch, A., eds., Arsenic in Ground Water; Geochemistry and Occurrence: Kluwer Academic Publishers, p. 127-176.
- Lapakko, K.A. 1999. Laboratory drainage quality from siltite-argillite rock (final Appendices for BLM contract J910C82009), Minnesota Department of Natural Resources, Minerals Division, St. Paul, MN 55155-4045, 1 March 1999, 6 Appendixes (A1-A6).
- Lapakko, K.A., and White, W.W., III. 2000. Modification of the ASTM 5744-96 kinetic test, in Proceedings from the Fifth International Conference on Acid Rock Drainage (ICARD 2000), Denver, Colorado, May 21-24, 2000, Volume I: Littleton, Colorado, Society for Mining, Metallurgy, and Exploration, Inc., p. 631-639.
- Morin, K.A., and Hutt, N.M. 1998. Kinetic tests and risk assessment for ARD: 5th Annual BC Metal leaching and ARD Workshop, December 9-10, Vancouver, Canada, 10 p.
- Morrison, J.M., Irwin, E.R., Lee, L., and Goldhaber, M.B. 2002. Historical geochemical and biological characterization of a southern Appalachian watershed impacted by coal acid mine drainage: Geological Society of America Annual Meeting, v. 34, no. 6, p. 143.
- Oman, C.L., Finkelman, R.B., Halili, N., Goldhaber, M.B. 1995. Anomalous trace element concentrations in coal from the Warrior Basin, Alabama: Geological Society of American, Abstracts with Programs, Southeastern Section, p. A78.
- Pashin, J.C. 1991. Regional analysis of the Black Creek-Cobb coalbed methane target interval, Black Warrior Basin, Alabama: Geological Survey of Alabama Bulletin 145, 127 p.
- Ridley, W.I. 2000. Instruction manual for "Quantlaser"; a batch process macro for reduction of quantitative laser ablation data: U.S. Geological Survey Open-File Report 00-0311, 42 p.

- Stoffregen, R.E., Alpers, C.N., and Jambor, J.L. 2000. Alunite-Jarosite Crystallography, Thermodynamics and Geochronology *in* Sulfate Minerals, Reviews in Minerals and Geochemistry, v. 40, p. 454-474. <http://dx.doi.org/10.2138/rmg.2000.40.9>
- Taylor, J.C. 1991. Computer programs for the standardless quantitative analysis of minerals using the full powder diffraction profile: Powder Diffraction, v. 6, p. 2-9. <http://dx.doi.org/10.1017/S0885715600016778>
- White, W.W., III, and Lapakko, K.A. 2000. Preliminary indications of repeatability and reproducibility of the ASTM 5744-96 kinetic test for drainage pH and sulfate release rate *in* Proceedings from the Fifth International Conference on Acid Rock Drainage, SME, Littleton, CO, p. 621-630.
- Wilson, S.A., Ridley, W.I., and Koenig, A.E. 2002. Development of sulfide calibration standards for the laser ablation inductively-coupled plasma mass spectrometry technique: Journal of Analytical Atomic Spectrometry, v. 17, p. 405-409. <http://dx.doi.org/10.1039/B108787H>